Population-wide evolution of SARS-CoV-2 immunity tracked by a ternary immunoassay

Marc Emmenegger[1], Elena De Cecco[1], David Lamparter[2,#], Raphaël P. B. Jacquat[3,4,#] Daniel Ebner[5], Matthias M. Schneider[3], Itzel Condado Morales[1], Dezirae Schneider[1], Berre Doğançay[1], Jingjing Guo[1], Anne Wiedmer[1], Julie Domange[1], Marigona Imeri[1], Rita Moos[1], Chryssa Zografou[1], Chiara Trevisan[1], Andres Gonzalez-Guerra[1], Alessandra Carrella[1], Irina L. Dubach[6], Catherine K. Xu[3], Georg Meisl[3], Vasilis Kosmoliaptsis[7,8], Tomas Malinauskas[9], Nicola Burgess-Brown[10], Ray Owens[9,11], Stephanie Hatch[5], Juthathip Mongkolsapaya[12], Gavin R. Screaton[12], Katharina Schubert[13], John D. Huck[14], Feimei Liu[14], Florence Pojer[15], Kelvin Lau[15], David Hacker[15], Elsbeth Probst-Müller[16], Carlo Cervia[16], Jakob Nilsson[16], Onur Boyman[16,17], Lanja Saleh[18], Katharina Spanaus[18], Arnold von Eckardstein[18], Dominik J. Schaer[6], Nenad Ban[13], Ching-Ju Tsai[19], Jacopo Marino[19], Gebhard F. X. Schertler[19,20], Jochen Gottschalk[21], Beat M. Frey[21], Regina Reimann[1], Simone Hornemann[1], Aaron M. Ring[14], Tuomas P. J. Knowles[3,4], Ioannis Xenarios[2,22], David I. Stuart[9], and Adriano Aguzzi[1*]

[1] Institute of Neuropathology, University of Zurich, 8091 Zurich, Switzerland

[2] Health2030 Genome Center. 9 Chemin des Mines, 1202 Geneva, Switzerland

[3] Centre for Misfolding Diseases, Department of Chemistry, University of Cambridge, Lensfield Road, Cambridge CB2 1EW, United Kingdom

[4] Cavendish Laboratory, Department of Physics, University of Cambridge, JJ Thomson Ave, Cambridge CB3 0HE, United Kingdom

[5] Target Discovery Institute, University of Oxford, OX3 7FZ, England

[6] Division of Internal Medicine, University Hospital Zurich, 8091 Zurich, Switzerland

[7] Department of Surgery, Addenbrooke's Hospital, University of Cambridge, Hills Road, Cambridge CB2 0QQ, United Kingdom

[8] NIHR Blood and Transplant Research Unit in Organ Donation and Transplantation, University of Cambridge, Hills Road, Cambridge CB2 0QQ, United Kingdom

[9] Division of Structural Biology, The Wellcome Centre for Human Genetics, University of Oxford, Headington, Oxford, OX3 7BN, UK

[10] Structural Genomics Consortium, University of Oxford, Oxford, OX3 7DQ, UK

[11] The Rosalind Franklin Institute, Harwell Campus, OX11 0FA, UK

[12] Nuffield Department of Medicine, Wellcome Trust Centre for Human Genetics, University of Oxford, Oxford, UK

[13] Department of Biology, Institute of Molecular Biology and Biophysics, ETH Zurich, Zurich, Switzerland

[14] Department of Immunobiology, Yale School of Medicine, New Haven, CT, USA

[15] Protein Production and Structure Core Facility, EPFL SV PTECH PTPSP, 1015 Lausanne, Switzerland

[16] Department of Immunology, University Hospital Zurich, 8091 Zurich, Switzerland

[17] Faculty of Medicine, University of Zurich, 8006 Zurich

[18] Institute of Clinical Chemistry, University Hospital Zurich, 8091 Zurich, Switzerland

[19] Department of Biology and Chemistry, Laboratory of Biomolecular Research, Paul Scherrer Institute, 5303 Villigen-PSI, Switzerland

[20] Department of Biology, ETH Zürich, 8093 Zürich, Switzerland

[21] Regional Blood Transfusion Service Zurich, Swiss Red Cross, 8952 Schlieren, Switzerland

[22]Agora Center, University of Lausanne, 25 Avenue du Bugnon, 1005 Lausanne

[#] equal contribution

*to whom correspondence should be addressed: adriano.aguzzi@usz.ch

Serological assays can detect anti-SARS-CoV-2 (SARS2) antibodies, but their sensitivity often comes at the expense of specificity. Here we used a Ternary Automated Blood Immunoassay (TRABI) to assess the IgG response against SARS2 in 3'815 prepandemic plasma samples and 126 virologically and/or clinically confirmed COVID-19 samples. Posterior probabilities were calculated from 3x8 measurements of logarithmically diluted samples against the ectodomain and the receptor-binding domain of the spike protein and the nucleoprotein. We then performed 429'624 assays on 17'901 blood samples from patients of the University Hospital Zurich and from healthy blood donors. We found seropositivity in 44 of 8'591 patients and in 26 of 5'388 blood donors from December 2019 to May 2020. Western blotting confirmed seropositivity in COVID samples but in none of the prepandemic samples. Solution-equilibrium measurements revealed immunodominant antibodies with nanomolar affinity in COVID samples, whereas prepandemic plasma showed lower affinities despite similar titers for individual SARS2 antigens. Hence, TRABI identifies seropositive individuals in large unselected cohorts, discriminates between SARS2 immunity and low-affinity crossreactivity, and is therefore suitable for large-scale nationwide screening campaigns.

Introduction

Within just a few months of the onset of the SARS-CoV-2 (henceforth SARS2) pandemic, several million cases and hundreds of thousands of fatalities from Corona Virus Disease (COVID) have been registered. It has also indirectly caused many more deaths by hijacking healthcare resources, thereby making them unavailable to patients suffering from other diseases. In addition, COVID has created profound economic distress for most travel-related industries. Finally, it has disrupted a plethora of industrial supply chains, resulting in a massive worldwide unemployment crisis that will undoubtedly cost many more human lives.

In order to alleviate the direct consequences of the SARS2 pandemic, governments and public healthcare agencies need granular and reliable data on the prevalence of infection, the incidence of new infections, and the spatial-temporal oscillations of these parameters within regions of interest. The acquisition of such data, however, is daunting and data are prone to misinterpretation [1]. Firstly, data needs to be acquired extremely rapidly. Secondly, their usefulness is dependent on being representative of large populations, meaning that they need to be acquired in massive numbers. Finally, the tolerance of false-positives and false-negatives must be extremely low in order to ensure an accurate estimation of the prevalence.

Intuitively, PCR-based diagnostics would seem suitable to fulfill the above criteria. However, practical experience has shown that this is not the case. The acquisition of representative diagnostic material for PCR has proven challenging, with deep nasal swabs being difficult to perform, uncomfortable for patients and potentially hazardous for medical personnel. Accordingly, the sensitivity of PCR diagnostics is often disappointing, with reported false-negative rates of 25% even under the best conditions [2].

Serological assays, on the other hand, address the adaptive immune responses of the host which are fundamental to limiting viral spread within individuals and populations. While they lag behind the viral infection, they can serve as both powerful epidemiological tools as well as useful clinical aids. Firstly, antibodies can be easily retrieved from many biological fluids, notably including venous and capillary blood. Secondly, antibodies typically persist for several months whereas the viral load in the upper respiratory tract frequently wane within weeks [3]. Importantly, immunological assays can be largely automated, and are thus suitable to mass screening of extremely large cohorts. This aspect is crucial since it provides a reliable readout of degree of immunity in a population, which is necessary for responsible easing of social restriction measures.

Representative testing of entire populations mandates fully automatable assays capable of outputting reliable results at extremely high rates and very low cost. Here we describe an assay that

fulfills these criteria. We have screened 17,901 samples for antibodies against three SARS2-related antigens: the ectodomain of the spike protein (S), its receptor-binding domain (RBD) and the nucleocapsid protein (NC), using SARS2 enzyme-linked immunoassays (ELISA) [4-6]. Samples included patients entering the University Hospital of Zurich (USZ) from December 2019 to the present (defined as “copandemic”; n=8’591), a cohort of patients treated at USZ between 2016 and 2018 (“prepandemic”; n=2’719), as well as 1’096 prepandemic and 5’388 copandemic samples from blood donors in Zurich and Lucerne. Our test cohorts were completed by well-annotated virologically and/or clinically confirmed patients with SARS2 infections (75 for USZ and 51 samples for blood donors). Our results paint a detailed picture of the spread of the pandemic within the greater Zurich area, and may be representative of other metropolitan areas with a highly mobile population served by large international airports.

Results

TRABI: a miniaturized high-throughput ELISA for multiple SARS2 antigens.

For the detection of seroconversion in tens of thousands of individuals who potentially acquired an infection with SARS2, it was crucial to maximize the specificity and sensitivity of our assay. Another paramount consideration was the ability to maintain a throughput of >4'000 samples/24h and minimize the costs of reagents and labor. We achieved these goals (1) by testing for multiple viral antigens, (2) by employing extensive automation including contactless fluid-handling, (3) by vastly reducing the reagent volumes and (4) by adopting advanced statistical techniques for data interpretation.

TRABI utilizes acoustic dispensing [7] to transfer nanoliter amounts of plasma into high-density 1536-well plates (total assay volume: 3 µl) and measures the IgG response against the SARS2 spike protein (S, amino acids 1-1208, constituting the ectodomain of the protein which initiates the interaction with ACE2 [8]), the receptor binding domain (RBD, amino acids 330-532), and the nucleocapsid protein (NC, amino acids 1-419) (**Fig. 1A**). Each sample was tested at eight consecutive two-fold dilution points (1:50 to 1:6400), and the resulting data were fitted to a sigmoidal curve by logistic regression. The inflection point (or $-\log(EC_{50})$) of each sigmoid was defined as the respective antibody titer.

As reference samples for assay establishment, we utilized a collective of 56 venous plasma samples drawn at various days post onset of symptoms (dpo) from 27 RT-qPCR confirmed patients suffering from COVID-19 and hospitalized at the University Hospital of Zurich (USZ, true positives), as well as 90 anonymized USZ samples from the prepandemic era (true negatives) (see **Table S1**). We then constructed receiver operating characteristic (ROC) curves to assess the assay quality for each antigen individually. Finally, we created a composite metric that integrates S/RBD/NC measurements using quadratic discriminant analysis (QDA). While each single antigen showed an excellent discrimination of negatives and positives on samples drawn at ≥14 dpo, the QDA model outperformed the individual antigen measurements at 7-13 dpo, where the emergence of an IgG response is expected to be variable (**Fig. 1B**). We therefore used the QDA modeling assumptions to infer the prevalence in large cohorts based on the distributional information of true negatives and true positives (details in Methods) using information gained from all three antigens.

To benchmark TRABI, we compared the results with an in-house high-throughput assay under development at the University of Oxford (optimizations ongoing at the time of data acquisition), the Roche Elecsys, the DiaSorin, the EuroImmun, and the Abbott systems (**Fig. 1C**), using 139

of 149 samples (10 were removed from the analysis because of insufficient sample volume to perform all tests). While TRABI scored best at early time points compared to others, all the assays used for comparison performed equally well, with 100% specificity at 100% sensitivity as assessed by this dataset of clearly limited size. We then plotted the samples drawn at multiple dpo for all individuals to assess the evolution of the IgG response. The results revealed a temporal pattern consistent with the gradual emergence of IgG antibodies within 14 dpo (**Fig. 1D**). The

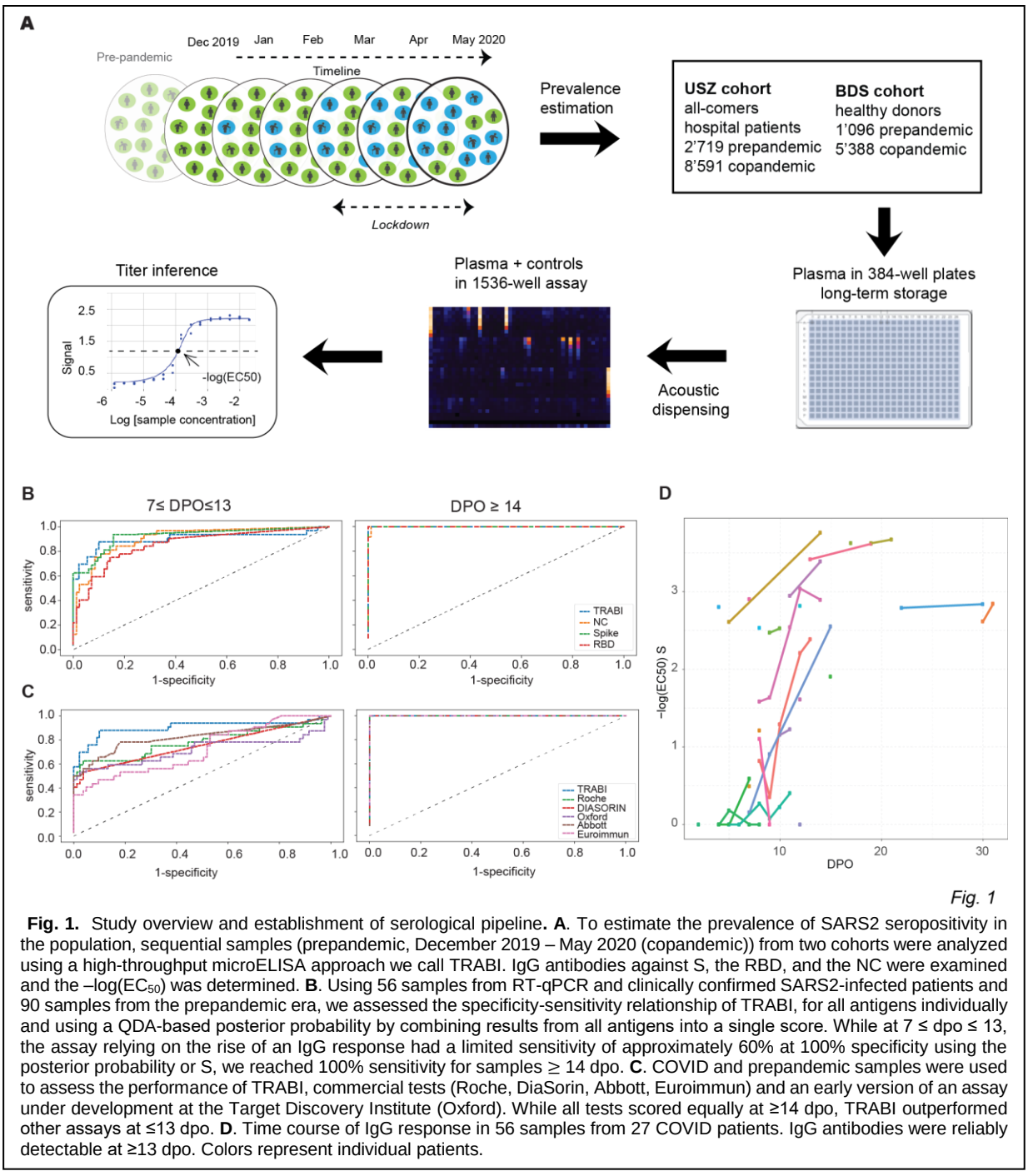

Fig. 1

Fig. 1. Study overview and establishment of serological pipeline**. A**. To estimate the prevalence of SARS2 seropositivity in the population, sequential samples (prepandemic, December 2019 – May 2020 (copandemic)) from two cohorts were analyzed using a high-throughput microELISA approach we call TRABI. IgG antibodies against S, the RBD, and the NC were examined and the –log(EC_{50}) was determined. **B**. Using 56 samples from RT-qPCR and clinically confirmed SARS2-infected patients and 90 samples from the prepandemic era, we assessed the specificity-sensitivity relationship of TRABI, for all antigens individually and using a QDA-based posterior probability by combining results from all antigens into a single score. While at 7 ≤ dpo ≤ 13, the assay relying on the rise of an IgG response had a limited sensitivity of approximately 60% at 100% specificity using the posterior probability or S, we reached 100% sensitivity for samples ≥ 14 dpo. **C**. COVID and prepandemic samples were used to assess the performance of TRABI, commercial tests (Roche, DiaSorin, Abbott, Euroimmun) and an early version of an assay under development at the Target Discovery Institute (Oxford). While all tests scored equally at ≥14 dpo, TRABI outperformed other assays at ≤13 dpo. **D**. Time course of IgG response in 56 samples from 27 COVID patients. IgG antibodies were reliably detectable at ≥13 dpo. Colors represent individual patients.

performance and throughput described above indicate that TRABI is suitable to investigate the prevalence of seroconversion at population scale.

Temporal evolution of SARS2 pandemics on the population level.

Due to supply-chain bottlenecks, but also because of the intrinsically narrow window of infectivity, testing of individuals for the presence of SARS2 nucleic acids is currently limited to those at elevated risk. In Switzerland, individuals with mild symptoms were asked to isolate at home, often without being tested for the presence of SARS2 RNA. Thus, the true number of people who underwent an infection with SARS2 may at best be a rough estimate modelled on data of PCR-confirmed cases and numbers of hospitalizations [9, 10]. We are therefore using TRABI to screen a large sample of Swiss urban populations. To date, we have screened 17,901 samples from a university hospital (USZ) cohort of individuals with diverse diseases (**Table S1**) and from the blood donation service (BDS, see **Table S1**) of Zurich and Lucerne (healthy group), starting from December 2019 (**Fig. S1A, B**).

To reliably measure the prevalence of seroconversion, we used known positives and negatives as internal calibrators for each cohort. We tested two models: the first model assumes that both the condition-positive and negative data follow distinct multivariate Gaussian distribution (**Fig. 2A, B**), whereas the second model assumes that condition-negative data follow a multivariate t distribution while condition positive follow again a Gaussian distribution (**Fig. S1C, D**). Within the USZ cohort, we queried the clinical records of all screened samples for the word “COVID” in anamnestic reports, for virologically confirmed SARS2 infection, or for solid clinical signs and symptoms of COVID. We annotated these samples and selected those with dpo ≥14, which we expected to have developed an IgG response, as condition-positive (n=19). To avail of condition-positives from the cohort of blood donors, 51 samples from convalescent individuals with PCR-confirmed SARS2 infection recruited for a plasmapheresis study were included. Importantly, we screened 3,815 prepandemic samples (condition-negatives) to determine potentially unspecific results, e.g. due to cross-reactivity with other coronaviruses. For the BDS cohort, we enriched the condition-negatives with 1,400 samples from December 2019 and January 2020 to increase the numbers of the assumed negatives and to obtain a more reliable baseline. Using the distributions of the condition negatives and the condition positives, we computed the posterior probability (i.e. the probability of an individual to be seropositive as modeled via the distribution of the known condition-negatives and known condition-positives) for all data points (see **Fig. S1A, B**). The respective ROC curves were then plotted (**Fig. S1E, F**). At 100% specificity, we identified 18/19 of the annotated true positives for the USZ (**Fig. S1E**) and 38/51 annotated true positives for the BDS cohort

(**Fig. S1F**). For the BDS cohort, the sensitivity increased rapidly with a slight decrease in specificity (at a false-positive-rate of 0.001, we identified 45/51 condition positives). We then applied this model to estimate the prevalence on the population level. No substantial shift above baseline was inferred for samples screened from January, February, and March 2020 (**Fig. 2C** and **Fig. S1G**, USZ cohort). A sudden increase in prevalence manifests in April (multivariate Gaussian: 0.8% (CI95%: 0.2%-1.4%) and multivariate t distribution: 0.4% (CI95%: 0.0%-0.8%)) and May 2020 (multivariate Gaussian: 1.3% (CI95%: 0.8%-1.8%) and multivariate t distribution: 0.9% (CI95%: 0.6%-1.4%)), in accordance with the virologically and clinically reported rise in SARS2 infections in these months. The assembly of healthy blood donors showed a comparable time course of seroconvertion, with the prevalence approximating 1% in April (multivariate Gaussian: 1.1% (CI95%: 0.6%-1.6%) and multivariate t distribution: 1.0% (CI95%: 0.5%-1.4%)) (**Fig. 2C** and **Fig. S1G**).

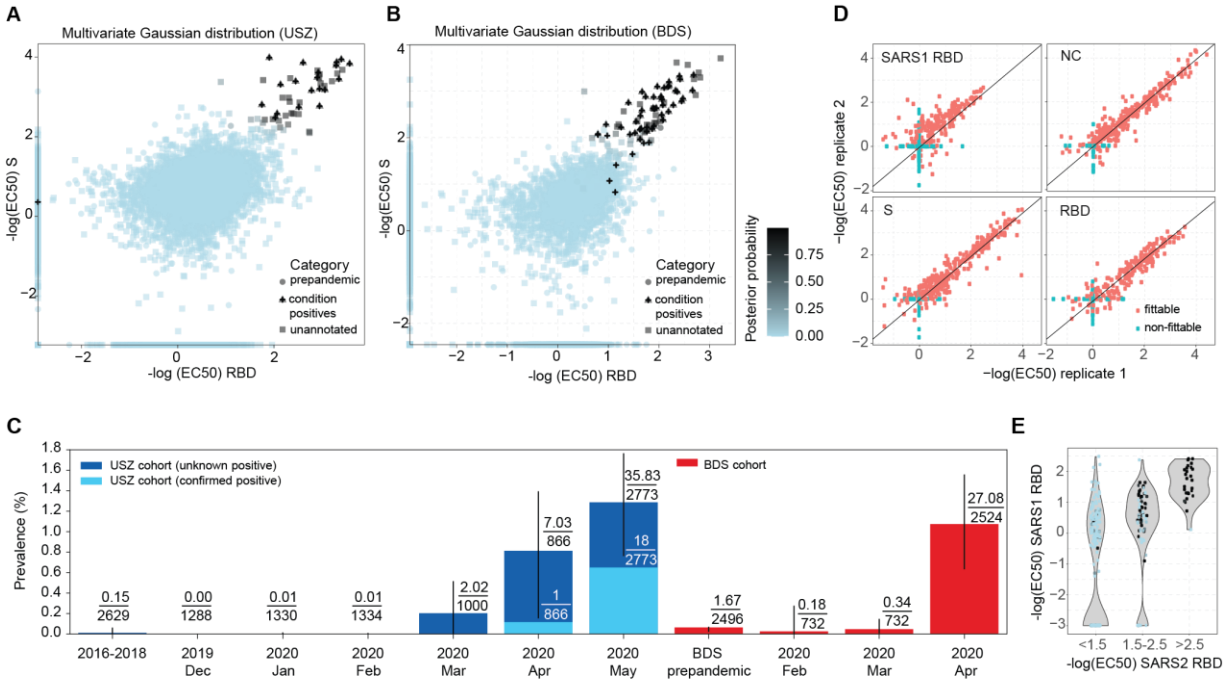

Fig. 2

Fig. 2. Evolution of SARS2 prevalence in a cohort of Zurich University Hospital (USZ) patients and donors from the blood donation service (BDS). **A-B**. Data points represent -log(EC_{50}) values of plasma titrated against S and the RBD in the USZ and BDS cohorts. Using QDA, the posterior probability was calculated assuming a multivariate Gaussian distribution. **C**. Prevalence of SARS2 seropositivity in prepandemic (before 2019) and co-pandemic samples (from December 2019 to May 2020) estimated using the posterior probabilities from the multivariate Gaussian distribution. Bar shows 95% CI. **D**. TRABI reproducibility was assessed using duplicates run in pairs of independent assay plates. **E**. To assess potential cross-reactivity of SARS2 seropositive individuals, we tested 210 high-scoring samples and 122 random samples for binding to the RBD of SARS1. SARS2 RBD binders with a high posterior probability (same color map as in B) segregated within the higher anti-SARS1-RBD titers.

To directly validate our method, we selected 210 high scoring samples and 122 random samples from known negatives and aimed to reproduce our results. The screens proved to be highly replicable when comparing the duplicates from the same screen (S: R^2 = 0.85 among samples where both could be adequately fitted, see **Fig. 2D**) and the values from the follow-up screen with the values initially derived from serology (for example, 87% among re-screened samples with a -logEC_{50} for S above 2.5 had a -logEC_{50} value above 2 in the second screen, see **Fig. S2**).

Antibodies against the RBD of SARS-CoV (henceforth termed SARS1) have shown to be able to bind to the RBD of SARS2 [11]. Here we included the SARS1 RBD to examine whether individuals with strong binding properties to the SARS2 RBD display cross-reactivity. For visualization, we formed groups that reflect the binding propensity of individuals to SARS2 RBD (<1.5; 1.5-2, > 2.5) and indicated their respective QDA-derived posterior probability. For individuals with SARS2 RBD < 2, a small fraction show binding to SARS1 RBD at –log(EC_{50}) > 2 (**Fig. 2E**). However, those with strong binding properties to SARS2 RBD (> 2.5) cluster at high values for SARS1 RBD, indicating that some anti-SARS2 RBD antibodies are likely cross-reactive to SARS1 RBD.

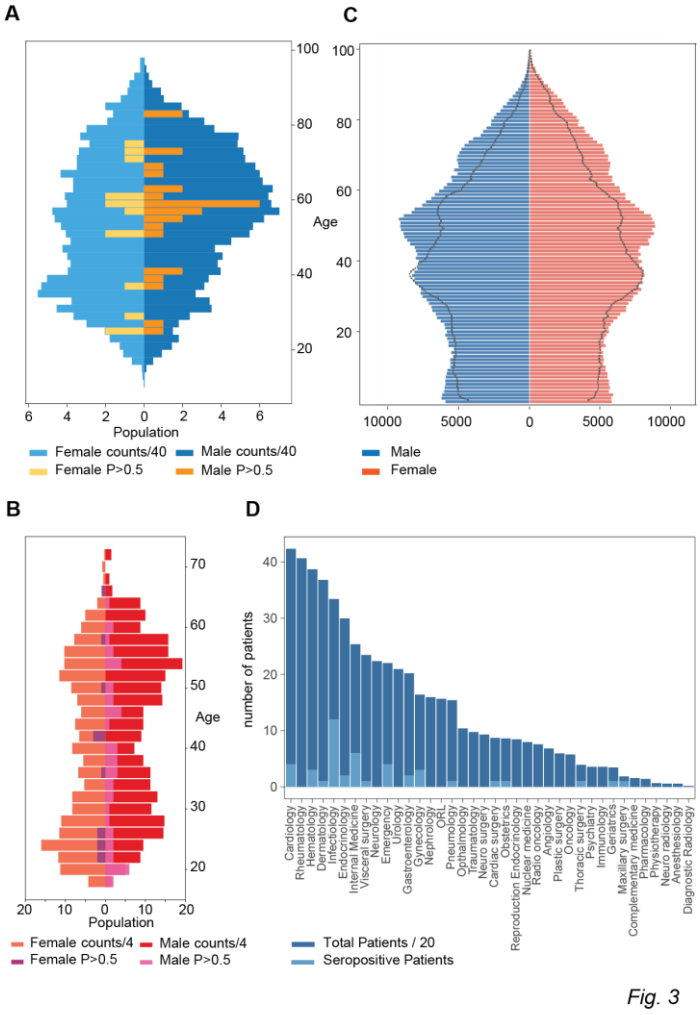

Fig. 3. Demographic and clinical annotations of the tested cohorts. **A**. and **B**. Age and gender pyramids for the USZ (A) and the BDS (B) cohorts with indications of the respective posterior probability (p > 0.5). **C**. Age pyramid of inhabitants of the Canton of Zurich. **D**. Distribution of plasma samples by hospital departments (total/20: dark blue; posterior probability > 0.5: light blue).

In summary, TRABI identified first cases of SARS2 seroconversion in April 2020, consistent with first infections reported in the Zurich area towards the end of February 2020. While data obtained

from healthy individuals suggest that around 1% of blood donors have been infected in the absence of clear clinical symptoms, the serological prevalence is about 5-fold higher than RT-qPCR confirmed cases for the same time point. However, these data indicate that seroconversion within the greater area of Zurich is still exceedingly rare and very far from herd immunity.

Clinical and demographic characteristics of serologically confirmed SARS2 infected hospital patients and healthy donors.

The USZ cohort had a median age of 56 (41 - 69) years, with a median of those with an increased posterior probability (> 0.5) of 59 (51 - 63) (**Fig. 3A** and **Table S1**). The BDS cohort had a median age of 43 (29 -54), while those individuals with posterior probability > 0.5 had a median age of 39 (29 - 53) (**Fig. 3B** and **Table S1**). **Fig. 3C** shows the age pyramid of the inhabitants of the Canton of Zurich [12], as a comparison to our cohorts. The blood of USZ patients was drawn in 38 clinical departments (**Fig. 3D**) of which 16 treated patients that we consider SARS2-positive based on a posterior probability > 0.5. In absolute counts, most SARS2-positive samples were obtained from Infectiology, followed by Internal Medicine, Cardiology and Emergency. The wide range of departments that sees SARS2-infected patients is indicative that SARS2 seropositive patients do not solely enter the hospital for the treatment of COVID-19 but for any condition that requires the attention of a USZ physician. Lastly, seropositivity can be found across all age groups and in both genders, with more male individuals affected in the USZ and BDS cohorts (**Fig. 3A**, **B**, **Table S1**). More time is needed to track and correlate SARS2 seropositivity with disease susceptibility.

Prevalence of anti-SARS2 antibodies in prepandemic samples.

5'215 prepandemic plasma samples (2'719 USZ hospital patients and 2'496 healthy BDS donors) were examined for the presence of cross-reactive antibodies against S, RBD and NC of SARS2. Several individuals had a strong antibody response against a single antigen and an absence of binding to other antigens (**Fig. S1A, B**). We then directly compared prepandemic and co-pandemic samples in the USZ cohort on the basis of single antigens and their respective posterior probabilities. When focusing on samples with high values for single assays, we observed an enrichment of high posterior probabilities in pandemic but not in the prepandemic group (**Fig. 4A**). Among samples with individual $-\log(EC_{50})$ values above 2 in May, 66% (S), 82% (RBD), and 17% (NC) had a posterior probability above 0.5. At the same time, no sample with an individual assay level above 2 had a posterior probability above 0.5 in the prepandemic samples. This enrichment

is suggestive of a substantial performance improvement when using the combined metric in the USZ cohort.

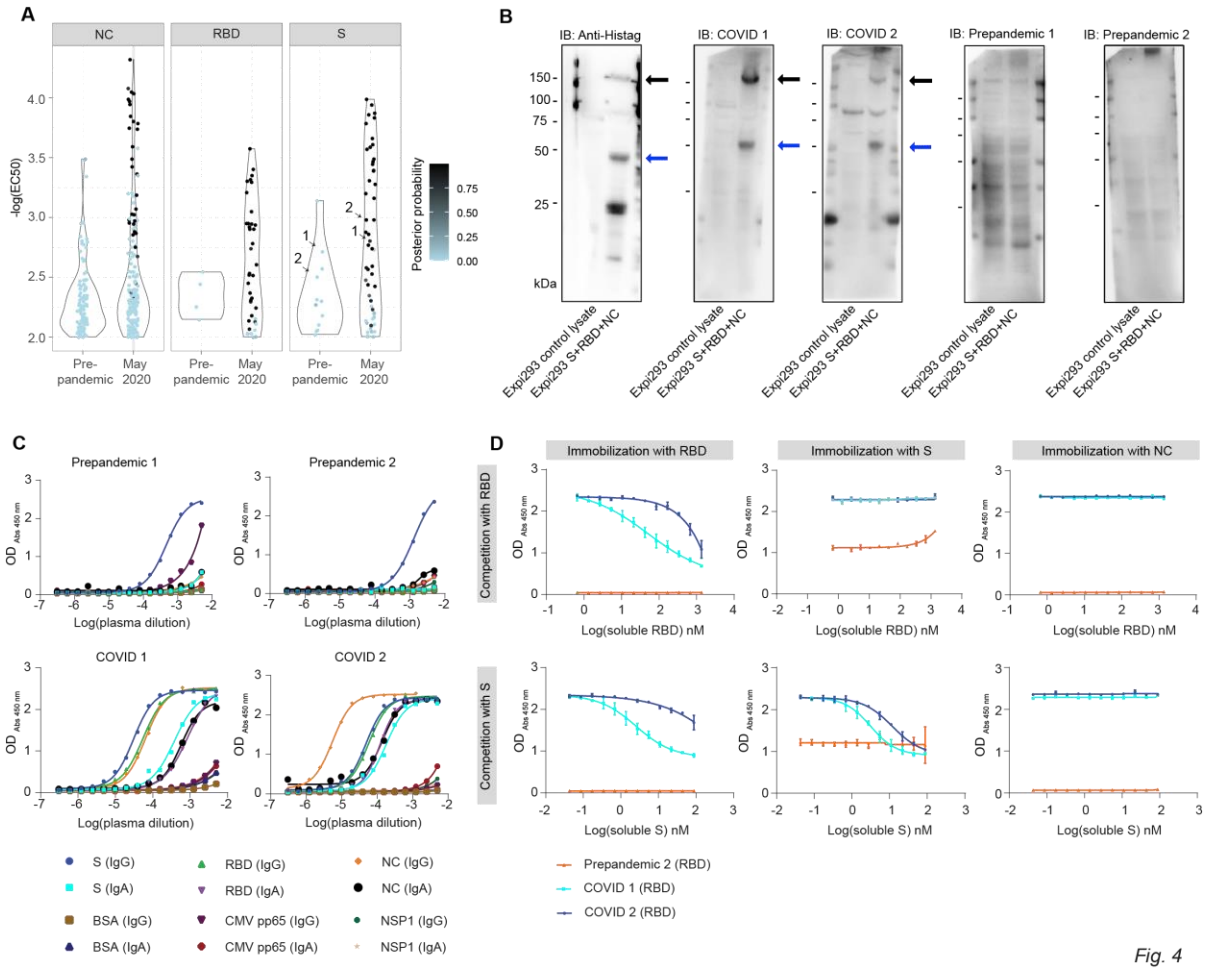

Fig. 4

Fig. 4. A. Posterior probability calculated using the Gaussian distribution, visualized for single antigens for prepandemic samples vs. USZ samples drawn in May 2020. Prepandemic samples exhibited a low posterior probability as they typically react against single antigens, leading to low rankings in a composite metric. For further testing, comparative samples were chosen from the prepandemic era and from May 2020. **B**. Western Blot analysis of two samples from May 2020 ("COVID 1" and "COVID 2") and two prepandemic samples ("prepandemic 1" and "prepandemic 2"). Anti-his-tag antibody was included as a positive control. Lane 1 = non-transfected Expi293F cell lysate; Lane 2 = Expi293F cell lysates expressing his-tagged S, NC and RBD proteins. Black arrows: S; blue arrows: NC. Uncropped images in Fig. S4. **C.** ELISA assays on the same samples as in B, using SARS2 S, NC, RBD and NSP1 as well as control proteins (BSA, CMV pp65). **D**. Soluble RBD or S were allowed to engage with plasma (same samples as in B and C), and ELISA was then performed with immobilized RBD or S. Data points represent averages of duplicates. Soluble antigens suppressed the ELISA signal in the COVID samples but not in the prepandemic sample, showing that the antibodies present in the latter had low affinities for the SARS2 targets.

We then compared the immunochemical properties of two prepandemic samples with high binding to S to two samples of confirmed COVID (COVID 1 and 2, see annotation in **Fig. 4A**). The COVID samples, but not the prepandemic samples, recognized in Western blots the S, RBD and NC antigens of SARS2 expressed by Expi293F (**Fig. 4B**). Additional ELISAs performed on the same samples confirmed the initial findings (**Fig 4C**) including binding to the RBD in COVID but not in

prepandemic samples. However, COVID samples showed reactivity in Western Blot against both S and NC, but not against RBD (**Fig. 4B**), suggesting that they recognized conformational epitopes lost upon boiling and SDS denaturation.

To probe the specificity of the findings, we also carried out competitive ELISAs on 3 out of 4 specimens including prepandemic and COVID patients. First, we determined plasma concentrations close to the EC_{50}. Then we pre-incubated appropriately diluted samples with various concentrations of S and RBD (0.04-88 and 0.7-1350 nM, respectively). Samples were then transferred onto ELISA plates coated with S, RBD, and NC. The concentration-dependent displacement of the measured optical density was then visualized (**Fig. 4D**). We found that both soluble S and the RBD caused a concentration-dependent depletion of the RBD in COVID samples, but not in a prepandemic sample. The prepandemic sample displayed no competition, suggesting that its reactivity was due to high concentrations of low-affinity antibodies cross-reacting with SARS2 S.

Identification of asymptomatic cases with TRABI and clonality of anti-S immune response.

TRABI enabled the identification of 26 blood donors with no apparent signs of SARS2 infection (**Fig. 2B**, **C**). They had no reported symptoms despite clear serological indications of past infection, as confirmed by ELISA (**Fig. 5A**). In a comparative approach, we investigated IgG and IgA antibodies to S, RBD, and NC as well as responses to multiple control antigens, in four asymptomatic blood donors and 4 convalescent individuals recruited to the BDS for a plasmapheresis study. We observed binding of IgG antibodies in asymptomatic and convalescent individuals against S, RBD, and NC, with usually lower IgA titers. No binding against the SARS2 non-structural-protein 1 (NSP1), or against bovine serum albumin (BSA) was observed. We confirmed these findings by using the samples of the asymptomatic and convalescent individuals as primary antibodies in Western Blot and detected bands for both S and the NC in the Expi293 cells overexpressing the viral proteins but not in the Expi293 control lysate (**Fig. 5B**).

To obtain a rough estimate of the clonality and epitope specificity of the immune response raised against the S protein, we conducted an ELISA-based soluble antigen competition. Competition with the RBD lead to a decrease in ELISA signal for RBD but not for S or NC (**Fig. 5C** and **Fig. S3A**). Conversely, competition with S decreased the signal for both S and the RBD (**Fig. 5C**), suggesting the presence of antibodies targeting multiple S epitopes, including RBD. Therefore, the immune response against S was polyclonal.

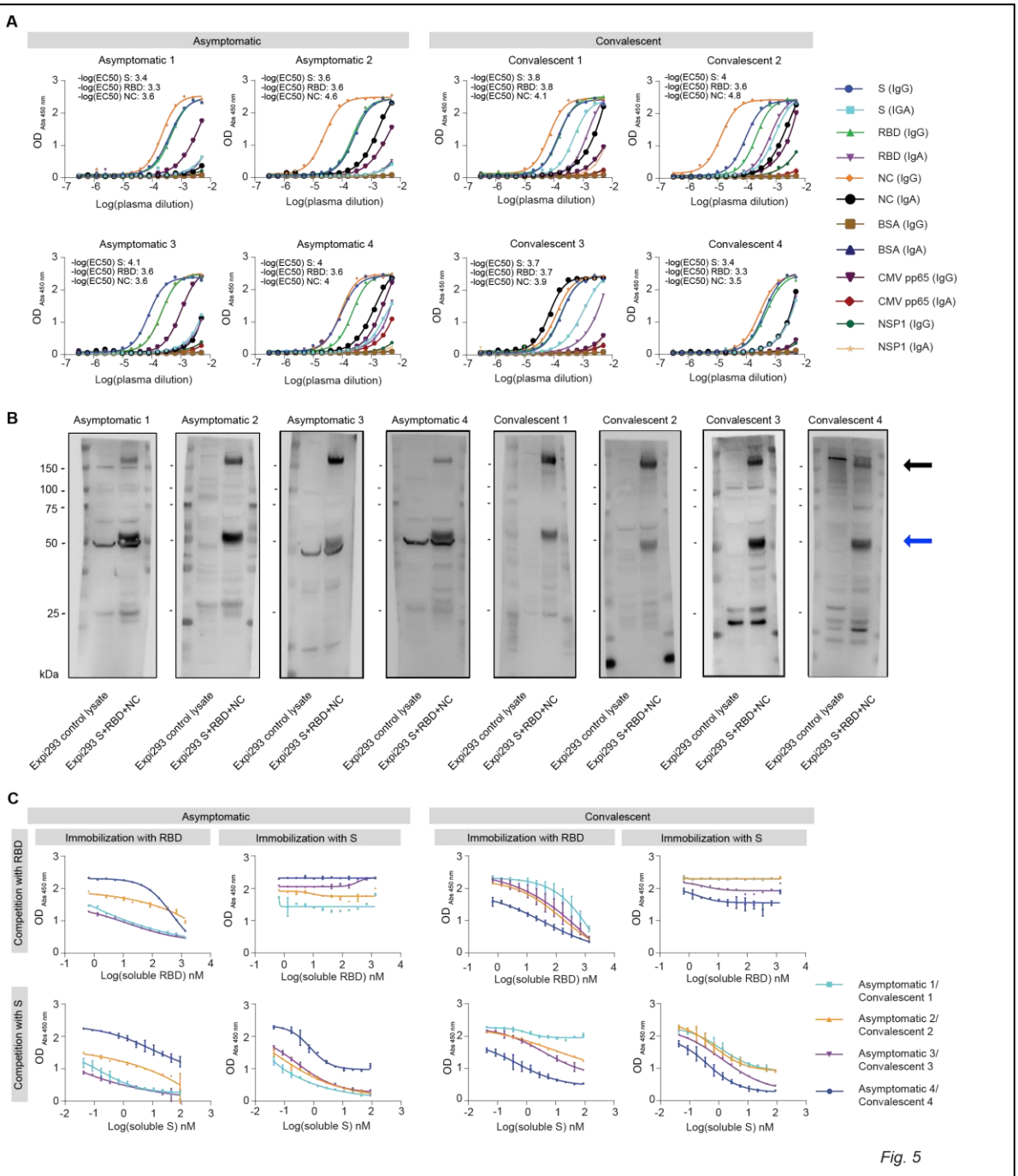

Fig. 5

Fig. 5. Clonality of anti-S immune response. **A**. ELISA assays of four asymptomatic and four convalescent individuals. **B**. Western Blot analysis of the same individuals tested in (A). Lane 1 = non-transfected Expi293F cell lysate; Lane 2 = Expi293F cell lysates expressing His-tagged S, His-tagged NC, His-tagged RBD proteins. Black arrows indicate S, while blue arrows point at NC. For a better visualization, brightness and contrast have been modified and the images have been partially cropped. The original images are shown in Fig. S4. **C**. Competitive ELISA using RBD or S for soluble competition with antibodies in plasma. The assay was performed on the four asymptomatic and four convalescent individuals tested in (A), (B) and (C). Each point is the average of two technical duplicates, with error bars. Data related to “asymptomatic 4” individual in the competitive ELISA using soluble RBD and immobilization for RBD (upper left graph) show only one replicate, as we encountered technical issues. All samples show a high reactivity against the antigens and display an overall similar behavior in terms of antigen competition. The differences in the antigen-mediated antibody depletion among the samples might be indicative of diverse immune responses.

Discussion

The high-throughput pipeline for SARS2 serology described above has enabled us to study a large cohort over a time span of six months, with up to 1'000 more samples being tested every day. In view of the critique levelled at past serological studies [1, 13], we have gone to great lengths to assess and validate our technology. For the initial assay calibration, sensitivity was measured using a panel of clinically and RT-qPCR confirmed SARS2 sera (n=56) at various time points after onset of clinical signs and symptoms and 90 negative controls. A blinded comparison with commercial test kits showed that our approach – combining three individual assays into one single score – was suitable for large-scale epidemiologic studies.

A key question for handling the current SARS2 pandemic is the true rate of people who have already contracted the virus. As a proxy for the estimation of the true prevalence in the population of the greater area of Zurich, we have used two independent cohorts: (1) unselected patients coming from all clinical departments of USZ and (2) healthy individuals donating blood to local blood banks (BDS). The availability of known positives and negatives in both cohorts allowed us to model the posterior probability from the multiple available antigen measurements in a principled way, using the respective distributions of the known negatives and positives. Enrichment of samples with high posterior probabilities in excess of the single assays during the pandemic phase, suggests that combining the metrics did indeed lead to a power gain. One drawback of modeling the multivariate distribution of antigen measurements directly, is that deviation from modeling assumption are harder to detect and correct in a multivariate situation. We explored the robustness-to modeling-assumption by modeling the condition negative samples, either with a multivariate Gaussian or multivariate t distribution and saw moderate drops in predicted prevalence when going from a Gaussian to t distribution (11% for BDS and 30% for USZ). An alternative would be to focus on linear methods that enable the data to be projected onto one dimension first, such as linear discriminant analysis, allowing the estimate of prevalence from a univariate mixture distribution. The extent of our sampling, however, bolsters our confidence in the representability and validity of our results.

We find that in both cohorts, the prevalence of seropositives continues to linger around 1%. Each of our cohorts entail intrinsic biases. On the one hand, the USZ cohort consists mostly of individuals suffering from diseases, some of which may be a consequence of SARS2 infections. On the other hand, individuals with acute infections are typically excluded from donating blood. As a consequence, the BDS cohort may be biased against individuals who may have experienced COVID symptoms and refrained from donating. Because of these fundamental differences in the

composition of the USZ and BDS cohorts, we find it particularly relevant that both cohorts converge towards a prevalence around 1%. This observation undescores the presumption that the prevalence reported here is truly representative of the population under study.

The low prevalence of SARS2 immunity is unexpected for many reasons. The initial trajectory of the disease with high replicative numbers had engendered suggestions that a large swath of the population might have encountered the virus and developed humoral immunity. This idea is now soundly refuted. The 1% prevalence is even more surprising when considering that (1) Switzerland borders on Northern Italy whose prevalence of infection was reported to reach 43% in healthcare workers [14], (2) Ticino and Western Switzerland were profoundly affected by the pandemic, and (3) no travel restrictions were imposed between Ticino and Northern Switzerland.

When set in relation to the regional numbers of RT-qPCR-positive cases, our cohort-based estimates of the seroprevalence (1% in early May 2020) are in line with those of more affected regions of Switzerland, like Geneva (seroprevalence around 9.7%, end of April 2020 [15]) and are about 5-10 times higher than the respective incidence of overt COVID [16].

A recent publication [17] has shown pre-existing anti-SARS2 antibodies in unexposed humans. Our affinity determinations and immunoblots, however, point to fundamental differences between prepandemic seropositivity and the immune responses of SARS2-infected individuals. While the latter consistently showed high-affinity responses that were clearly visible in Western blotting, the few seropositive prepandemic sera were mostly negative in Western blotting, and equilibrium displacement ELISA of one prepandemic plasma sample suggested a much lower affinity despite similar antibody EC_{50} titers. We conclude that any immune response in uninfected individuals, whether it represents cross-reactivity with common-cold coronaviruses or something else, is of inferior quality and may be less likely to be protective.

Our population-wide screen allows us to address several crucial questions that have been controversially discussed. What is the frequency of truly asymptomatic cases? What is the complete spectrum of clinical signs and symptoms with which SARS2-infected individuals present? Many SARS2 patients present with monosymptomatic anosmia, and it is conceivable that other illnesses may represent hitherto unrecognized signs of SARS2 infection. Stratifying the results of our screens, e.g. by referencing clinic and by ICD codes and laboratory values of the patients, will become increasingly important in the years to come, e.g. to protect those at risk, to evaluate immune defenses and their possible waning, and to plan vaccination campaigns.

Our study is conceived as a long-term exercise which, given appropriate funding, will be continued for the next several years. In addition to allowing precise monitoring of the population, it will also

enable the determination of titer decays in seropositive individuals as a function of demographic indicators and of comorbidities. However, there are societal concerns linked to antibody testing, and scientists must not downplay them. Serology is a powerful medical and epidemiological instrument, but it can also be misused to stratify the workforce, to discriminate against the non-immune, and even for far more nefarious deeds. Let's study immune responses, but let's not create a dystopian society based on them.

Materials and Methods

Human specimens and data

All experiments and analyses involving samples from human donors were conducted with the approval of the local ethics committee (KEK-ZH-Nr. 2015-0561, BASEC-Nr. 2018-01042, and BASEC 2020-00802), in accordance with the provisions of the Declaration of Helsinki and the Good Clinical Practice guidelines of the International Conference on Harmonisation. Specimens were denoted according to the following conventions: *prepandemic samples*: samples collected before December 2019; *COVID samples*: samples from patients with clinically and/or virologically confirmed SARS2 infection; *co-pandemic samples*: any samples collected in December 2019 or thereafter.

Sample acquisition and biobanking

Small volumes (< 100 µL) of heparin plasma samples were obtained from the Institute of Clinical Chemistry at the University Hospital of Zurich as unique bio specimens, biobanked over recent years in a high-throughput liquid biobank. We received one sample per patient per month. After one month, another sample from the same individual would be included. EDTA plasma from healthy donors was obtained from the Blutspendedienst (blood donation service) Kanton Zürich and Kanton Luzern from donors who signed the consent that their samples can be used for conducting research.

High-throughput serological screening.

In order to test the samples for the presence of IgG antibodies directed against SARS-CoV-2 antigens, high-binding 1536-well plates (Perkin Elmer, SpectraPlate 1536 HB) were coated with 1 µg/mL S or RBD or NC in PBS at 37 °C for 1 h, followed by 3 washes with PBS-T (using Biotek El406) and by blocking with 5% milk in PBS-T (using Biotek MultifloFX peristaltic pumps) for 1.5 h. Three µL plasma, diluted in 57 µL sample buffer (1% milk in PBS-T), were dispensed at various volumes (from 1200 nL down to 2.5 nL) into pre-coated 1536-well plates using contactless dispensing with an ECHO 555 Acoustic Dispenser (Labcyte/Beckman Coulter). Sample buffer was filled up to 3 uL total well volume using a Fritz Gyger AG Certus Flex dispenser. Thereby, dilution curves ranging from plasma dilutions 1:50 to 1:6400 were generated (eight dilution points per patient plasma sample). After the sample incubation for 2 h at RT, the wells were washed five times with wash buffer and the presence of IgGs directed against above-defined SARS-CoV-2 antigens was detected using an HRP-linked anti-human IgG antibody (Peroxidase AffiniPure Goat Anti-Human IgG, Fcγ Fragment Specific, Jackson, 109-035-098, at 1:4000 dilution in sample buffer). The incubation of the secondary antibody for one hour at RT was followed by three

washes with PBS-T, the addition of TMB, an incubation of three minutes at RT, and the addition of 0.5 M H2SO4 (both steps with Biotek MultifloFX syringe technology). The final well volume for each step was 3 µL. The plates were centrifuged after all dispensing steps, except for the addition of TMB. The absorbance at 450 nm was measured in a plate reader (Perkin Elmer, EnVision) and the inflection points of the sigmoidal binding curves were determined using the custom designed fitting algorithm described below.

Counter screening using commercial and custom-designed platforms

We used the following commercial tests for the detection of anti-SARS-SARS2 antibodies in 56 plasma samples of 27 patients who were diagnosed by RT-PCR to be infected by SARS-SARS2 as well as 83-90 plasma samples which were collected before December 2019 and, hence, before the start of the COVID19 pandemics: The double-antigen sandwich electro-chemiluminescence immunoassay from Roche diagnostics (Rotkreuz, Switzerland) was performed with the E801 of the COBAS8000® system (Roche diagnostics, Rotkreuz, Switzerland). The test detects any antibody against the nucleocapsid antigen. The fully automated LIAISON® SARS-CoV-2 chemiluminescence immunoassay from DiaSorin (Saluggia, Italy) detects IgG against the S1/S2 antigens. The SARS-CoV-2 chemiluminescent microparticle immunoassay from Abbott (Abbott Park, IL, USA) detects IgG against the nucleocapsid antigen and was performed on an Architect™ analyser. Two ELISAs from EUROIMMUN (Lübeck, Germany) detect IgA or IgG against the S1 antigen and were performed by the use of a DSX™ Automated ELISA System (DYNEX Technologies (Chantilly, VA, USA). The high-throughput serology assay in Oxford (under development) was carried out in the Target Discovery Institute, University of Oxford. High-binding 384-well plates (Perkin Elmer, SpectraPlate) were coated with 20 µL of 2.5 µg/mL S o/n at 4°C, followed by 3 washes with PBS-T and by blocking with 5% milk in PBS-T for 2 h. Blocking buffer was removed and 20 µL of 1:25 sera diluted in sample buffer (1% milk in PBS-T) was dispensed into S-coated wells then incubated for 2 h at RT. The wells were washed five times with wash buffer and the presence of IgGs directed against S was detected using an HRP-linked anti-human IgG antibody (Peroxidase AffiniPure Goat Anti-Human IgG, Fcγ Fragment Specific, Jackson, 109-035-098) at 1:50,000 dilution in 20 µL sample buffer. The incubation of the secondary antibody for one hour at RT was followed by three washes with PBS-T and the addition of QuantaRed™ Enhanced Chemifluorescent HRP Substrate Kit (Thermo Scientific, Waltham Massachusetts, USA) then incubated for four minutes at RT before the addition of the stop solution. The fluorescence at excitation/emission maxima of ~570/585nm was measured in a fluorescent plate reader (Perkin Elmer, EnVision).

Data analysis.

Data fitting. Data fitting. Eight-dilution points equally spaced on a logarithmic scale are fitted with an equation derived from a simple binding equilibrium. The inflection point (-$\log_{10}EC_{50}$) is extracted from the fit. Baseline and plateau values are fixed by the respective positive and negative controls in a plate-wise fashion and the signal is fitted following these equations:

$$c_{bound} = 1 - \frac{1}{2}\left(c_a c + k_d + 1 - \sqrt{(c_a c + k_d)^2 + 2(k_d - c_a c) + 1}\right) \ ,$$

where c_{bound} , c_a and c are concentration of the antigen-antibody, antigen, and blood concentration respectively.

$$\mathrm{OD}_{\mathrm{signal}} = c_{bound}\,(baseline - plateau) + plateau$$

Data preprocessing. All samples that yielded an $-\log_{10}EC_{50}$ of below –3 on any antigen were labelled as non-fittable and non-detectable. Their dilution curves cannot be differentiated from baseline and therefore only an upper bound for the $-\log_{10}EC_{50}$ can be determined. These samples were therefore excluded from data fitting but were of course included in ROC analysis and prevalence estimation.

QDA and Prevalence estimation. Assume that we have data for m samples with known serostatus and antibody measurements, that is, we have $(X_i, Y_i), i = 1, .., m,$ where X_i is the vector of size p (in our case our antigen measurements) and Y_i is a Boolean variable defining group membership (in our case, whether the individual is seropositive or not). The QDA model assumes multivariate normal distributed X_i given Y_i:

$$(X|Y = j) \sim \mathcal{N}_p\left(\mu_j, \Sigma_j\right).$$

Further, the model assumes that the prior, that is, distribution of Y_i , is known s. t. $P[Y = j] = \pi_j$

The quadratic discriminant classifier simply assigns each sample to the group which has the larger posterior $P[Y|X]$, which is proportional to the joint probability $P[Y, X]$.

Therefore, we assign sample i to group 1 if

$$\log(f_{x|y=1}(x_i)) + \log(\pi_1) > \log(f_{x|y=0}(x_i)) + \log(\pi_0),$$

And to group 0 otherwise. To set the prior, one option is to take just the mean of the group sizes. However, this is not an ideal option in our case, where we have an additional n samples with unknown serostatus to classify: The prevalence in the m samples with known serostatus might deviate substantially from the prevalence in population with unknown serostatus. We therefore estimate $\pi_1$directly from the data of unknown serostatus using a simple expectation maximization scheme. Proceeding in an iterative fashion, from a given estimate π_1^k, we define the posterior (E step):

$$t_1^k(x_i) = \frac{\pi_1^k f_{x|y=1}(x_i)}{\pi_1^k f_{x|y=1}(x_i) + (1-\pi_1^k) f_{x|y=0}(x_i)}.$$

Then, we update our estimate of π_1 (M step):

$$\pi_1^{k+1} = \frac{t_1^k(x_i)}{n}.$$

After convergence, this yields our estimate of the positive serostatus prevalence in the samples. Note that the sample ordering according to this classifier is independent of the prior and therefore has no impact on an analysis via ROC curves. Further, note that evaluating QDA via ROC analysis, an out of sample scheme should be employed to avoid biased estimates of performance; we chose 10-fold cross-validation throughout. Lastly, note that the strategy does not critically depend on the normality assumption but just requires an estimate for the density functions, $f_{x|y=j}(x_i)$. Even nonparametric estimates could be an option. We either restricted $f_{x|y=j}$ both to multivariate Gaussian or set $f_{x|y=0}$to a multivariate t with estimated degrees of freedom while still modeling $f_{x|y=1}$as Gaussian. For degrees of freedom estimation, we used the R package *QRM*. 95% confidence intervals were derived by bootstrap drawing 1000 bootstrap samples.

High-throughput validation screen

For the validation screen, we picked 60 and 150 samples from BDS and USZ respectively, that had the highest average values when summing -logEC_{50} for both Spike and RBD. Additionally, we added 52 and 70 randomly selected prepandemic samples for the BDS and the USZ cohort respectively. We supplemented the three antigens used in the first screen (NC, S, RBD of SARS-

SARS2) with a SARS-CoV RBD antigen. Unlike for the primary screen, we ran all samples in duplicates spread over two independent plates.

Protein production

The proteins were produced and purified at different sites in Zurich (CH), Oxford (UK), Lausanne (CH), and Yale University (USA).

Oxford, SGC. Recombinant proteins were purified as reported previously with small modifications [6, 18]. Mammalian expression vectors containing secreted, codon-optimized SARS-CoV-2 S (pHL-Sec [19]; aa. 1-1208, C-terminal 8His-Twin-Strep) and RBD (pOPINTTGNeo; aa. 330-532, C-terminal 6His) were transiently transfected with linear PEI into Expi239™ cells cultured in roller bottles in FreeStyle 293 media. Cell culture media was harvested after 3 days at 37°C for RBD or 3 days at 30°C for Spike and then buffered to 1X PBS. Proteins were first pulled down on Ni^{2+} IMAC Sepharose® 6 Fast Flow (GE) with stringent washing (>50 CV with 40 mM imidazole). RBD was polished on a Superdex 75 16/600 column (GE) equilibrated with 1X PBS, while Spike was directly dialyzed into 1X PBS using SnakeSkin™ 3,500 MWCO dialysis tubing. Proteins were concentrated with VivaSpin® centrifugal concentrators, centrifuged at 21,000 x *g* for 30 min to remove precipitates, and flash frozen at 1 mg/mL

Lausanne, EPFL SV PTECH PTPSP and Zurich UZH. The prefusion ectodomain of the SARS-CoV-2 S protein (the construct was a generous gift from Prof. Jason McLellan, University of Texas, Austin; see [18]) was transiently transfected either into suspension-adapted ExpiCHO cells (Thermo Fisher) or Expi293F (Thermo Fisher) cells with PEI MAX (Polysciences) in ProCHO5 medium (Lonza). After transfection, incubation with agitation was performed at 31°C and 4.5% CO2 for 5 days. The clarified supernatant was purified in two steps; via a Strep-Tactin XT column (IBA Lifesciences) followed by Superose 6 10/300 GL column (GE Healthcare) and finally dialyzed into PBS. The average yield was 15 mg/L culture.

Yale, New Haven. Human codon optimized SARS-CoV (2003) RBD (pEZT containing H7 leader sequence; aa. 306-527, C-terminal Avi- and 8His tags) was transiently transfected into Expi293™ cells (Thermo Fisher) using the ExpiFectamine™ 293 Transfection kit (Gibco) according to the manufacturer's instructions. Cells were cultured in a 37˚C incubator with 8% humidified CO_2 for 4 days after transfection. Culture supernatant was collected by centrifugation (500 x g for 10 minutes) and RBD was captured using Ni-NTA Superflow resin (Qiagen), washed, and eluted in buffer containing 50 mM Tris-HCl pH 8, 350 mM NaCl, and 250 mM imidazole. RBD was further purified using an ENrich™ SEC 650 column (Bio-Rad) equilibrated in 1X PBS (Thermo Fisher). Peak fractions were pooled and the protein concentration was determined by 280 nm absorbance

with a Nanodrop™ One Spectrophotometer (Thermo Fisher). Protein was snap frozen in liquid nitrogen and shipped on dry ice prior to experiments.

Zurich, ETH. NSP1 carrying an N-terminal His6-tag followed by a TEV cleavage site was expressed from a pET24a vector. The plasmid was transformed into E. coli BL21-CodonPlus (DE3)-RIPL and cells were grown in 2xYT medium at 30 °C. At an OD600 of 0.8, cultures were shifted to 18 °C and induced with IPTG to a final concentration of 0.5 mM. After 16 h, cells were harvested by centrifugation, resuspended in lysis buffer (50 mM HEPES-KOH pH 7.6, 500 mM KCl, 5 mM MgCl2, 40 mM imidazole, 10% (w/v) glycerol, 0.5 mM TCEP and protease inhibitors) and lysed using a cell disrupter (Constant Systems Ltd). The lysate was cleared by centrifugation for 45 min at 48.000 xg and loaded onto a HisTrap FF 5-ml column (GE Healthcare). Eluted proteins were incubated with TEV protease at 4 °C overnight and the His6-tag, uncleaved NSP1 and the His6-tagged TEV protease were removed on the HisTrap FF 5-ml column. The sample was further purified via size-exclusion chromatography on a HiLoad 16/60 Superdex75 (GE Healthcare), buffer exchanging the sample to the storage buffer (40 mM HEPES-KOH pH 7.6, 200 mM KCl, 40 mM MgCl2, 10% (w/v) glycerol, 1 mM TCEP). Fractions containing NSP1 were pooled, concentrated in an Amicon Ultra-15 centrifugal filter (10-kDa MW cut-off), flash-frozen in liquid nitrogen, and stored until further use at -80 °C.

Details of viral proteins used for this study

For *high-throughput serology*, the following proteins were used: SARS-CoV-2 S (pHL-Sec; aa. 1-1208, C-terminal 8His-Twin-Strep) and RBD (pOPINTTGNeo; aa. 330-532, C-terminal 6His) produced at the SGC in Oxford and the nucleocapsid protein from AcroBiosystems (AA Met 1 - Ala 419, C-terminal his-tag, NUN-C5227). For *competitive ELISA*, we used: The prefusion ectodomain of the SARS-CoV-2 S protein (Lausanne, EPFL SV PTECH PTPSP), the RBD from Trenzyme (C-terminal his-tag, P2020-001) and the nucleocapsid protein from AcroBiosystems (AA Met 1 - Ala 419, C-terminal his-tag, NUN-C5227). For *additional ELISAs* following the high-throughput serology, we used: The prefusion ectodomain of the SARS-CoV-2 S protein (Lausanne, EPFL SV PTECH PTPSP), the RBD from Trenzyme (C-terminal his-tag, P2020-001) and, nucleocapsid protein from AcroBiosystems (AA Met 1 - Ala 419, C-terminal his-tag, NUN-C5227), the SARS2 NSP1 protein (from Nenad Ban, ETH Zurich), the CMV pp65 protein (Abcam, ab43041), and BSA (Thermo Scientific).

Western Blotting

Expi293F cells were obtained as a gift from Prof. Maurizio Scaltriti (Memorial Sloan Kettering Cancer Center, New York). Non transfected control cells and cells overexpressing either His-

tagged S, His-tagged NC or His-tagged RBD domain were lysed in 0,1% Triton X-100/PBS. Total protein content in the cellular fraction was quantified using bicinchoninic protein assay (Pierce BCA Protein Assay Kit, ThermoFisher). For Western Blotting, 30 µg of ECD-expressing lysate, 10 µg of NC-expressing lysate and 10 µg of RBD-expressing lysate were loaded all in the same well of NU-PAGE 4-12% Bis-Tris gels (ThermoFisher). 50 µg of non-transfected cell lysate were loaded as negative control. Gels were run at a constant voltage (150 V) in MES running buffer for 50 minutes, then transferred onto PVDF membrane with a dry transfer system (iBlot 2 Gel Transfer Device, ThermoFisher). The membranes were blocked with 5% SureBlock (Lubio Science) for 1 hour at room temperature, and then incubated overnight with a 1:100 dilution of patients' plasma in 1% SureBlock, at 4 degrees. The day after, membranes were washed four times with PBS-T and incubated for 1 hours with an anti-human secondary antibody, HRP-conjugated, diluted 1:10000 in 1% SureBlock. The membranes were then washed four times with PBS-T and acquired using Immobilon Crescendo HRP Substrate (Merck Millipore) and Fusion SOLO S imaging system (Vilber). As a positive control, one membrane was incubated overnight with mouse anti-Histag antibody (ThermoFisher, dilution 1:10000 in 1% SureBlock) and subsequently with anti-mouse secondary antibody, HRP-conjugated (Jackson, dilution 1:10000 in 1% SureBlock).

Competitive ELISA

To perform competitive ELISAs, high-binding 384-well plates (Perkin Elmer, SpectraPlate 384 HB) were coated with 1 ug/mL S or RBD or NC in PBS at 37°C for 1 h, followed by 3 washes with PBS-T and by blocking with 5% milk in PBS-T for 1.5 h. Meanwhile, plasma samples were diluted to a final concentration close to the EC_{50}, incubated with either RBD (50 ug/mL) or S (12.5 ug/mL) and serially diluted (11 dilution points per patient sample, 25 uL per dilution) in a low-binding 384-well plates (Perkin Elmer, high binding SpectraPlate). After 2 h of incubation at RT, 20 uL of all the samples were transferred to the previously coated plates and incubated for additional 2 h at RT. Then, the plates were washed five times with PBS-T and the presence of IgGs was detected using an HRP-linked anti-human IgG antibody (Peroxidase AffiniPure Goat Anti-Human IgG, Fcγ Fragment Specific, Jackson, 109-035-098, at 1:4000 dilution in sample buffer). The incubation of the secondary antibody for one hour at RT was followed by three washes with PBS-T, the addition of TMB, an incubation of 5 minutes at RT, and the addition of 0.5 M H2SO4. The absorbance at 450 nm was measured in a plate reader (Perkin Elmer, EnVision) and the inflection points of the sigmoidal binding curves were determined using a custom designed fitting algorithm.

References

1. Bendavid, E., et al., *COVID-19 Antibody Seroprevalence in Santa Clara County, California.* 2020: p. 2020.04.14.20062463.
2. Kucirka, L.M., et al., *Variation in False-Negative Rate of Reverse Transcriptase Polymerase Chain Reaction-Based SARS-CoV-2 Tests by Time Since Exposure.* Ann Intern Med, 2020.
3. He, X., et al., *Temporal dynamics in viral shedding and transmissibility of COVID-19.* Nat Med, 2020. **26**(5): p. 672-675.
4. Amanat, F., et al., *A serological assay to detect SARS-CoV-2 seroconversion in humans.* Nat Med, 2020.
5. Okba, N.M.A., et al., *Severe Acute Respiratory Syndrome Coronavirus 2-Specific Antibody Responses in Coronavirus Disease 2019 Patients.* Emerg Infect Dis, 2020. **26**(7).
6. Stadlbauer, D., et al., *SARS-CoV-2 Seroconversion in Humans: A Detailed Protocol for a Serological Assay, Antigen Production, and Test Setup.* Curr Protoc Microbiol, 2020. **57**(1): p. e100.
7. Krystufek, R. and P. Sacha, *Increasing the throughput of crystallization condition screens: Challenges and pitfalls of acoustic dispensing systems.* MethodsX, 2019. **6**: p. 2230-2236.
8. Song, W., et al., *Cryo-EM structure of the SARS coronavirus spike glycoprotein in complex with its host cell receptor ACE2.* PLoS Pathog, 2018. **14**(8): p. e1007236.
9. Salje, H., et al., *Estimating the burden of SARS-CoV-2 in France.* Science, 2020.
10. Lourenco, J., et al., *Fundamental principles of epidemic spread highlight the immediate need for large-scale serological surveys to assess the stage of the SARS-CoV-2 epidemic.* 2020: p. 2020.03.24.20042291.
11. Tai, W., et al., *Identification of SARS-CoV RBD-targeting monoclonal antibodies with cross-reactive or neutralizing activity against SARS-CoV-2.* Antiviral Res, 2020. **179**: p. 104820.
12. *Alter der Wohnbevoelkerung der Stadt Zuerich*. 2020 31.05.2020]; Available from: https://www.stadt-zuerich.ch/prd/de/index/statistik/publikationen-angebote/publikationen/webartikel/2018-07-11_Alter-der-Wohnbevoelkerung_die-Stadt-Zuerich-im-Vergleich.html.
13. Streeck, H., et al., *Infection fatality rate of SARS-CoV-2 infection in a German community with a super-spreading event.* 2020: p. 2020.05.04.20090076.
14. Sandri, M.T., et al., *IgG serology in health care and administrative staff populations from 7 hospital representative of different exposures to SARS-CoV-2 in Lombardy, Italy.* 2020: p. 2020.05.24.20111245.
15. Stringhini, S., et al., *Repeated seroprevalence of anti-SARS-CoV-2 IgG antibodies in a population-based sample from Geneva, Switzerland.* 2020: p. 2020.05.02.20088898.
16. BAG, *Coronavirus Krankheit 2019 (COVID-19): Situationsbericht zur epidemiologischen Lage in der Schweiz und im Fürstentum Liechtenstein. (Version 28.05.2020).* 2020.
17. Ng, K., et al., *Pre-existing and de novo humoral immunity to SARS-CoV-2 in humans.* 2020: p. 2020.05.14.095414.
18. Wrapp, D., et al., *Cryo-EM structure of the 2019-nCoV spike in the prefusion conformation.* Science, 2020. **367**(6483): p. 1260-1263.
19. Aricescu, A.R., W. Lu, and E.Y. Jones, *A time- and cost-efficient system for high-level protein production in mammalian cells.* Acta Crystallogr D Biol Crystallogr, 2006. **62**(Pt 10): p. 1243-50.

Acknowledgments

All authors wish to thank their entire teams for support in the lab. We thank Linda Irpinio for help in the lab. We thank Vishalini Emmenegger (ETH Zurich) for insightful advice and kind help with illustrations. We are grateful to Elisabeth J. Rushing (USZ) for proofreading the manuscript. We thank Guido Bucklar, Michael Fetzer, Patrick Hirschi, Katie Kalt, Karin Edler and Roland Naef (USZ) for their continuous help with hospital data, and Didier Trono for helpful insights and discussions. Above all, we are grateful to all blood donors and hospital patients for helping us conduct this study.

Funding

Institutional core funding by the University of Zurich and the University Hospital of Zurich to AA, as well as Driver Grant 2017DRI17 of the Swiss Personalized Health Initiative to AA. The robotic rig was acquired with a R'Equip grant of the Swiss National Foundation to AA. Screening methodologies had been developed thank to the support of an Advanced Grant of the European Research Council and a Distinguished Scientist Award of the Nomis Foundation to AA. Funding by grants of Innovation Fund of the University Hospital Zurich to AA, AvE, DS, EPM, ME, and OB. Access to the Creoptix WAVEsystem was kindly provided by Creoptix AG. Wädenswil, CH. This work was supported by ETH Research Grant ETH-23 18-2 and a Ph.D. fellowship by Boehringer Ingelheim Fonds to KS. Raphaël Jacquat acknowledges funding by the EPSRC for Doctoral Training in Sensor Technologies and Applications (grant EP/L015889/1). ICM acknowledges funding by the Swiss Government FCS. Carlo Cervia was funded by a Swiss Academy of Medical Sciences fellowship (#323530-191220). GFXS was supported by an COVID-19 Emergency Fund of the Director of PSI. TM is supported by Cancer Research UK grants C20724/A14414 and C20724/A26752 to Christian Siebold (Oxford). Oxford work was supported by the MRC and Chinese Academy of Medical Sciences Innovation Fund for Medical Science, China Grant 2018-I2M-2-002. GRS is supported as a Wellcome Trust Senior Investigator (grant 095541/A/11/Z) and receives funding from the National Institute for Health Research Biomedical Research Centre Funding Scheme.

Author contributions

Collected and processed the biological specimens, prepared and carried out the high-throughput screenings, maintained the machines: ME, DS, BD, JG, AW, MI, JD, CZ. Analyzed data from the high-throughput serology: DL, RJ, IX, ME, AA. Carried out follow-up ELISAs and competitive ELISAs: EDC, RM, ME. Carried out Western Blots: EDC, CT, AGG. Carried out and interpreted the affinity determinations (not shown in the current version of the manuscript): MMS, ICM, CKX,

GM, TJPK, VK, AA. Collected samples from COVID-19 patients for the establishment of serology: ILD, DJS. Coordinated the sample acquisition and processing from the Institute of Clinical Chemistry: AvE and LS. Coordinated the sample acquisition and processing from the blood donation services: BF and JG. Coordinated and performed high-throughput ELISAs for comparison in Oxford: DE, StH, DIS. Coordinated and performed SARS2 serological assays using commercial platforms: LS, KS, AvE, EPM, OB. Produced proteins: DIS, NBB, RO, TM, FP, DH, KL, EDC, JDH, FL, AMR, SH, GS. Coordinated the correspondence with the ethics committee of the Kanton of Zurich: RR, JN, ME. Produced and redacted the figures: AA, RJ, DL, EDC, ME. Conceived the idea of creating a biobank of plasma samples, supervised the study on a daily basis, proposed primary and confirmatory experiments, advised on best lab practices, on control experiments and on data interpretation: AA. Wrote abstract, introduction and discussion: AA. Wrote a first draft of the Results part of the manuscript: ME. Advised on and corrected the Results section: AA.

Competing interests

TPJK is a member of the board of directors of Fluidic Analytics. AA is a member of the board of directors of Mabylon AG which has funded antibody-related work in the Aguzzi lab in the past. All other authors declare no competing interests.

Data and materials availability

The raw data underlying this study will be made available upon reasonable request. The biobank samples are limited and were exhausted in several instances. Therefore, while we will make efforts to provide microliter amounts of samples to other researchers, their availability is physically limited.

Supplementary Materials:

Fig. S1. **A**. and **B**. Half-violin plots showing the distribution of anti-S/RBD/NC reactivity in the –log(EC_{50}) scale for the USZ (A) and the BDS (B) cohort. **C.** and **D**. Depicted are all the –log(EC_{50}) values calculated for S and the RBD for the USZ (C) and the BDS (D) cohort. Using QDA, the posterior probability was calculated assuming a multivariate t distribution. **E**. and. **F**. ROC curves for the USZ (E) and BDS (F) cohorts using the prepandemic samples (including the ones from December 2019 and January 2020 for BDS) as condition negatives and selected condition positives from both cohorts. **G**. Using the posterior probabilities from the multivariate t distribution, the prevalence of SARS2 seropositivity was calculated in prepandemic samples and then from December 2019 to May 2020. Data shows that while binding against the SARS2 antigens occurs in prepandemic samples, they entail a low posterior probability as the binding is confined to single antigens.

Fig. S2. Assay reproducibility using 210 high scoring samples and 122 random samples (based on results from the high-throughput screen) for binding against S, the RBD, and the NC **A.** S binding shows that reproducibility increases at higher values, consistent with increased posterior probabilities. **B.** Same observation as (A) for the RBD. **C**. Same observation as (A) for the NC.

Fig. S3. Competitive ELISA probing for NC signal.

Fig. S4. Uncropped and unmodified camera-acquired images of the Western Blots displayed in Fig. 4 and Fig. 5.

Table S1. Descriptive statistics of age and sex for all cohorts.

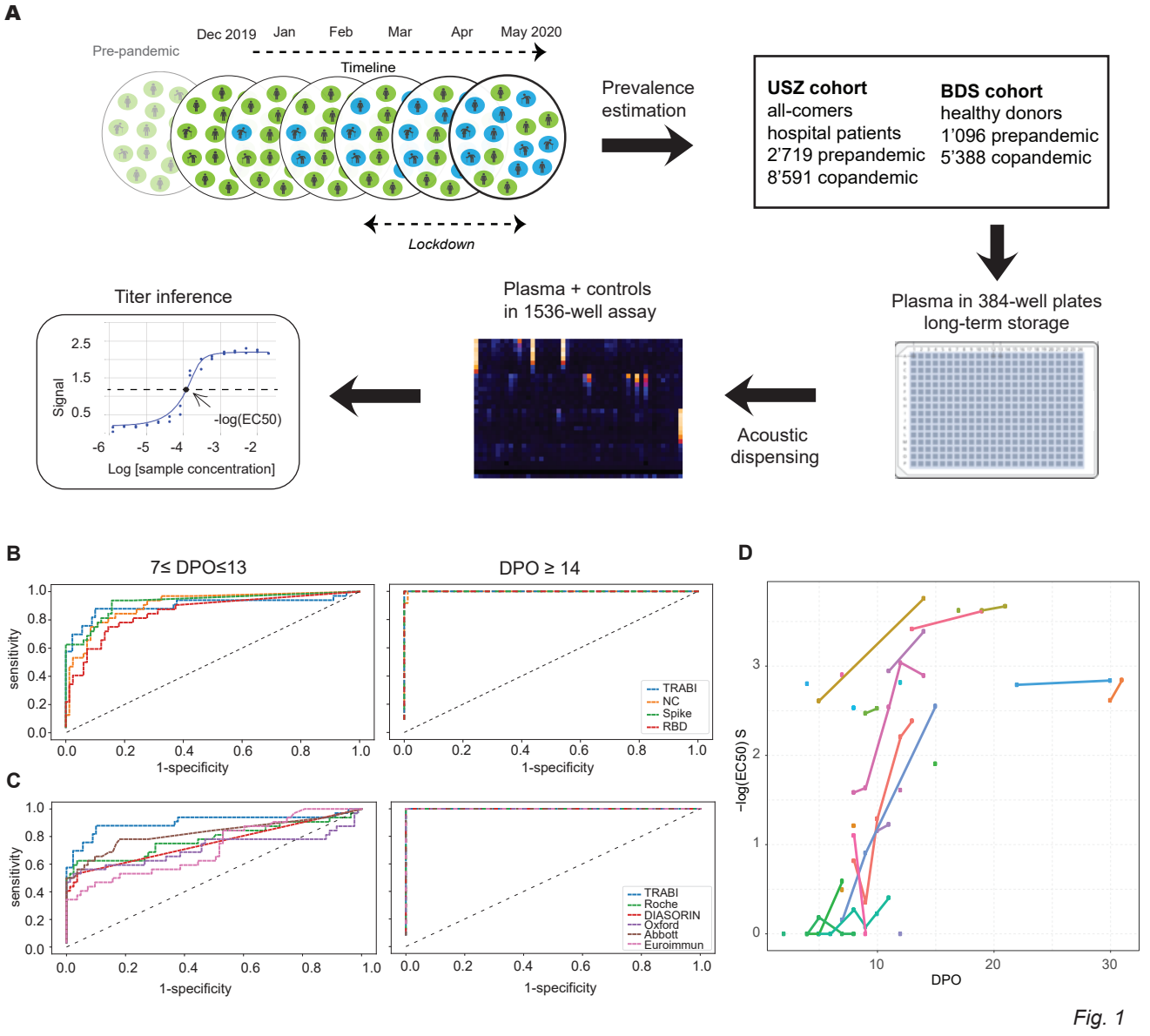
A
Pre-pandemic
Dec 2019
Jan
Feb
Mar
Apr
May 2020
Timeline
Lockdown
Prevalence estimation
USZ cohort
all-comers
hospital patients
2'719 prepandemic
8'591 copandemic
BDS cohort
healthy donors
1'096 prepandemic
5'388 copandemic
Plasma in 384-well plates
long-term storage
Acoustic dispensing
Plasma + controls
in 1536-well assay
Titer inference
Signal
-log(EC50)
Log [sample concentration]
B
7≤ DPO≤13
DPO ≥ 14
sensitivity
1-specificity
TRABI
NC
Spike
RBD
C
TRABI
Roche
DIASORIN
Oxford
Abbott
Euroimmun
D
−log(EC50) S
DPO

Fig. 1

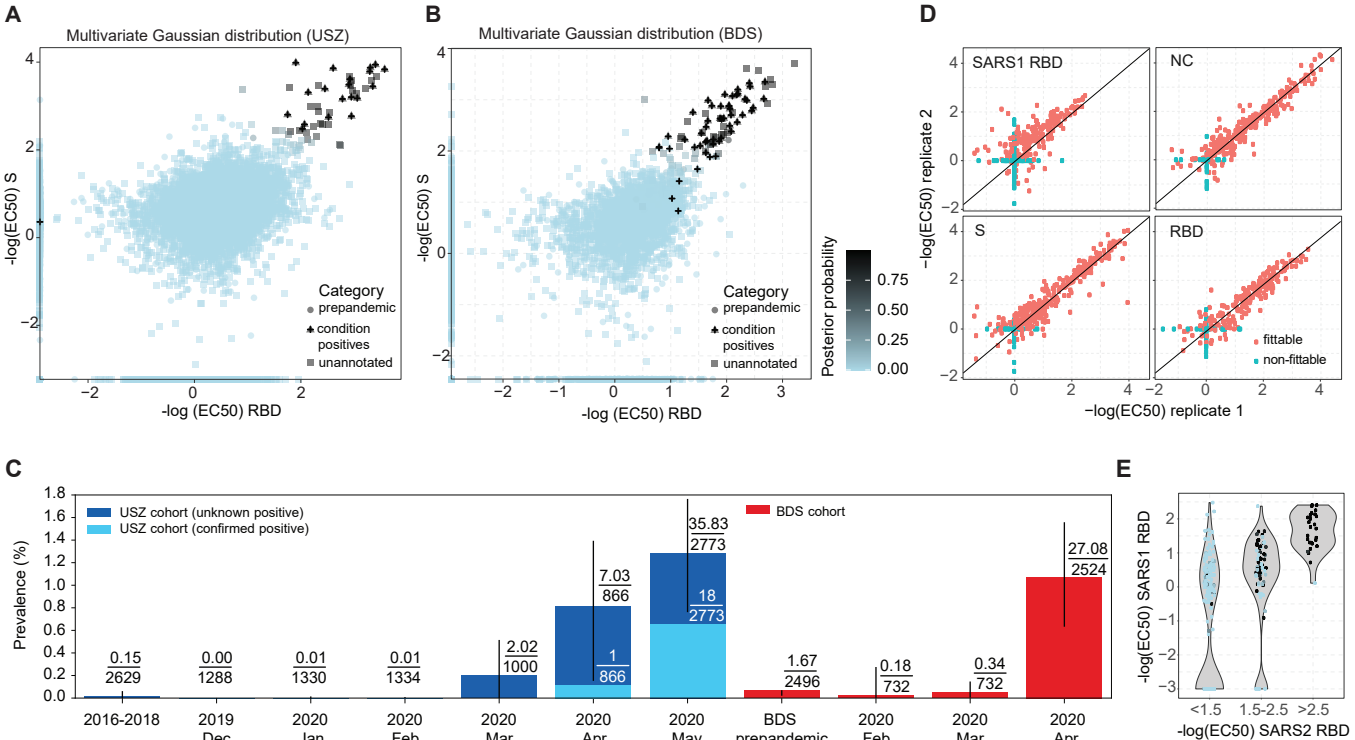
A
Multivariate Gaussian distribution (USZ)
-log(EC50) S
-log (EC50) RBD
Category
prepandemic
condition positives
unannotated
B
Multivariate Gaussian distribution (BDS)
-log(EC50) S
-log (EC50) RBD
Category
prepandemic
condition positives
unannotated
Posterior probability
0.75
0.50
0.25
0.00
D
SARS1 RBD
NC
S
RBD
−log(EC50) replicate 2
−log(EC50) replicate 1
fittable
non-fittable
C
Prevalence (%)
USZ cohort (unknown positive)
USZ cohort (confirmed positive)
BDS cohort
0.15 2629
0.00 1288
0.01 1330
0.01 1334
2.02 1000
7.03 866
1 866
35.83 2773
18 2773
1.67 2496
0.18 732
0.34 732
27.08 2524
2016-2018
2019 Dec
2020 Jan
2020 Feb
2020 Mar
2020 Apr
2020 May
BDS prepandemic
2020 Feb
2020 Mar
2020 Apr
E
-log(EC50) SARS1 RBD
<1.5
1.5-2.5
>2.5
-log(EC50) SARS2 RBD

Fig. 2

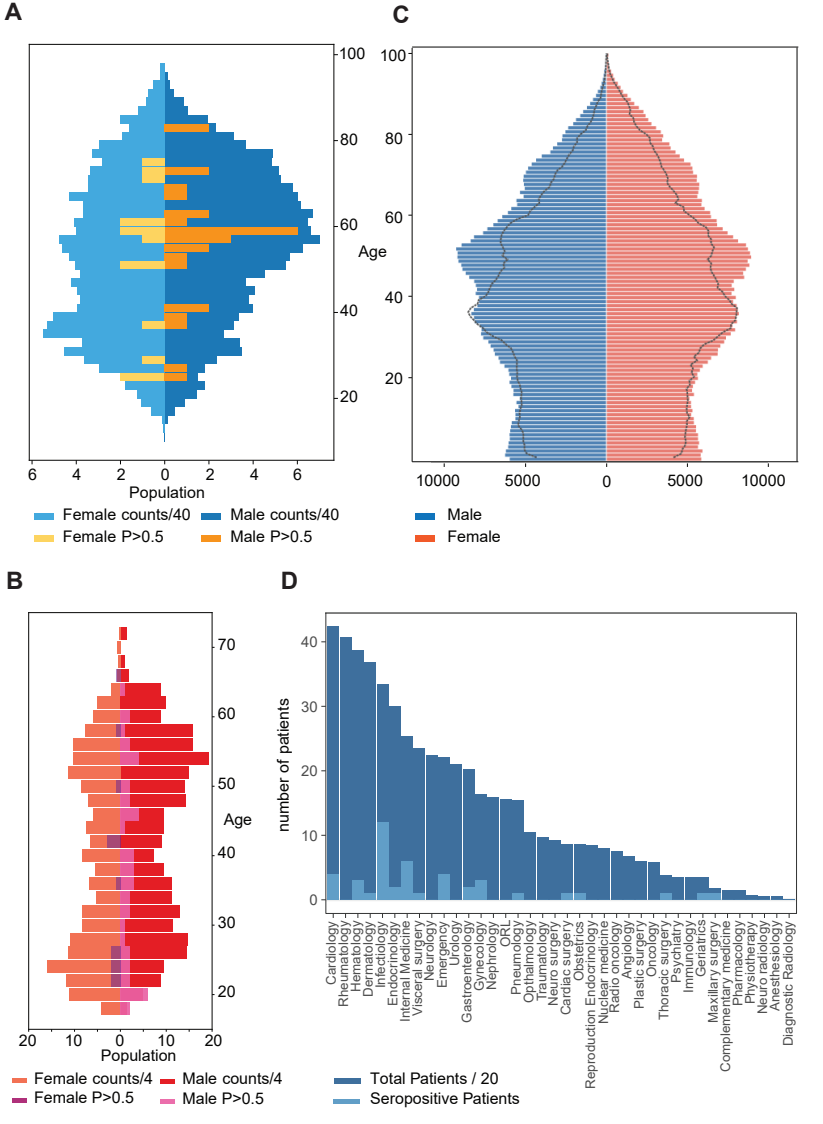
A
C
B
D
Age
Population
Female counts/40
Male counts/40
Female P>0.5
Male P>0.5
Male
Female
Female counts/4
Male counts/4
Female P>0.5
Male P>0.5
number of patients
Total Patients / 20
Seropositive Patients
Cardiology
Rheumatology
Hematology
Dermatology
Infectiology
Endocrinology
Internal Medicine
Visceral surgery
Neurology
Emergency
Urology
Gastroenterology
Gynecology
Nephrology
ORL
Pneumology
Ophthalmology
Traumatology
Neurosurgery
Cardiac surgery
Obstetrics
Reproduction Endocrinology
Nuclear medicine
Radio oncology
Angiology
Plastic surgery
Oncology
Thoracic surgery
Psychiatry
Immunology
Geriatrics
Maxillary surgery
Complementary medicine
Pharmacology
Physiotherapy
Neuro radiology
Anesthesiology
Diagnostic Radiology

Fig. 3

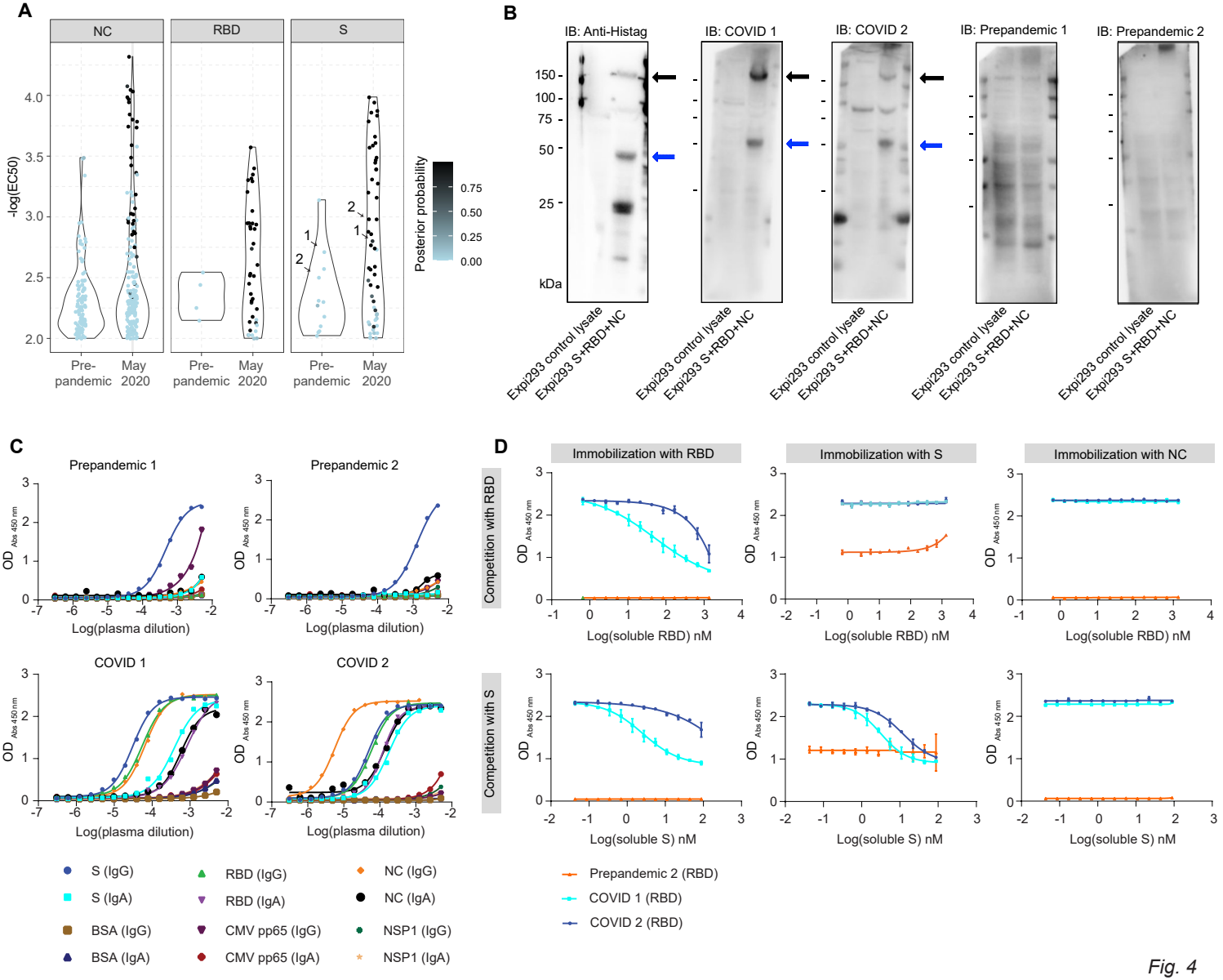
A
NC
RBD
S
-log(EC50)
Pre-pandemic
May 2020
Posterior probability
B
IB: Anti-Histag
IB: COVID 1
IB: COVID 2
IB: Prepandemic 1
IB: Prepandemic 2
kDa
Expi293 control lysate
Expi293 S+RBD+NC
C
Prepandemic 1
Prepandemic 2
COVID 1
COVID 2
OD Abs 450 nm
Log(plasma dilution)
S (IgG)
S (IgA)
BSA (IgG)
BSA (IgA)
RBD (IgG)
RBD (IgA)
CMV pp65 (IgG)
CMV pp65 (IgA)
NC (IgG)
NC (IgA)
NSP1 (IgG)
NSP1 (IgA)
D
Immobilization with RBD
Immobilization with S
Immobilization with NC
Competition with RBD
Competition with S
Log(soluble RBD) nM
Log(soluble S) nM
Prepandemic 2 (RBD)
COVID 1 (RBD)
COVID 2 (RBD)

Fig. 4

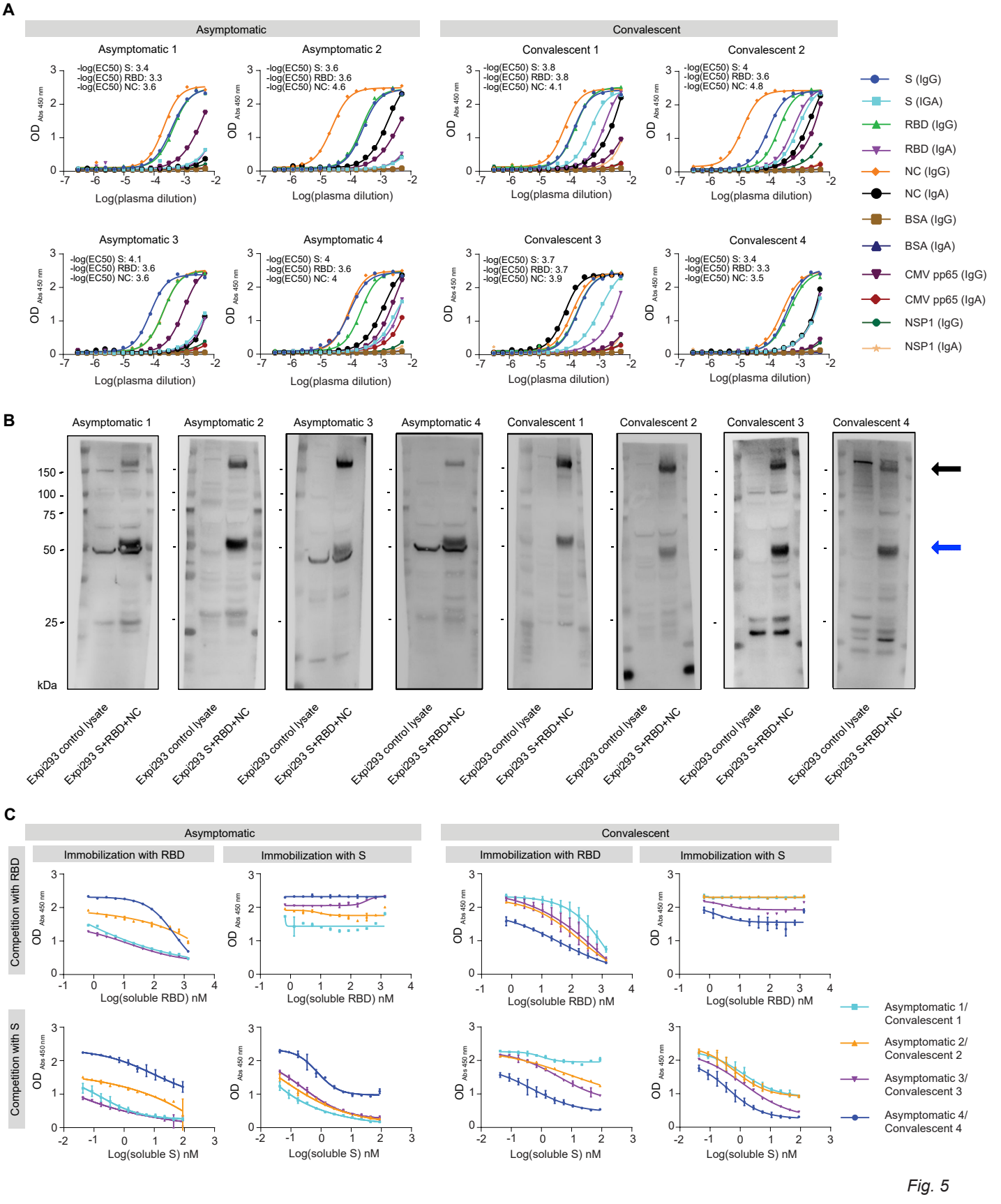
A
Asymptomatic
Convalescent
Asymptomatic 1
-log(EC50) S: 3.4
-log(EC50) RBD: 3.3
-log(EC50) NC: 3.6
Asymptomatic 2
-log(EC50) S: 3.6
-log(EC50) RBD: 3.6
-log(EC50) NC: 4.6
Convalescent 1
-log(EC50) S: 3.8
-log(EC50) RBD: 3.8
-log(EC50) NC: 4.1
Convalescent 2
-log(EC50) S: 4
-log(EC50) RBD: 3.6
-log(EC50) NC: 4.8
Asymptomatic 3
-log(EC50) S: 4.1
-log(EC50) RBD: 3.6
-log(EC50) NC: 3.6
Asymptomatic 4
-log(EC50) S: 4
-log(EC50) RBD: 3.6
-log(EC50) NC: 4
Convalescent 3
-log(EC50) S: 3.7
-log(EC50) RBD: 3.7
-log(EC50) NC: 3.9
Convalescent 4
-log(EC50) S: 3.4
-log(EC50) RBD: 3.3
-log(EC50) NC: 3.5
OD Abs 450 nm
Log(plasma dilution)
S (IgG)
S (IGA)
RBD (IgG)
RBD (IgA)
NC (IgG)
NC (IgA)
BSA (IgG)
BSA (IgA)
CMV pp65 (IgG)
CMV pp65 (IgA)
NSP1 (IgG)
NSP1 (IgA)
B
Asymptomatic 1
Asymptomatic 2
Asymptomatic 3
Asymptomatic 4
Convalescent 1
Convalescent 2
Convalescent 3
Convalescent 4
150
100
75
50
25
kDa
Expi293 control lysate
Expi293 S+RBD+NC
C
Asymptomatic
Convalescent
Immobilization with RBD
Immobilization with S
Competition with RBD
Competition with S
OD Abs 450 nm
Log(soluble RBD) nM
Log(soluble S) nM
Asymptomatic 1/
Convalescent 1
Asymptomatic 2/
Convalescent 2
Asymptomatic 3/
Convalescent 3
Asymptomatic 4/
Convalescent 4

Fig. 5